


Effect of dimensionality on the vortex dynamics in a type-II superconductorHemanta Kumar Kundu,¹ Kazi Rafsanjani Amin²,³ John Jesudasan³,³ Pratap Raychaudhuri³,³ Subroto Mukerjee,¹ and Aavek Bid^{1,*}¹*Department of Physics, Indian Institute of Science, Bangalore 560012, India*²*University Grenoble Alpes, CNRS, Grenoble INP, Institut Néel, 38000 Grenoble, France*³*Tata Institute of Fundamental Research, Mumbai 400005, India* (Received 7 August 2019; revised manuscript received 17 October 2019; published 1 November 2019)

We explore the effects of sample dimensionality on vortex pinning in a type-II, low- T_C , s -wave superconductor, NbN, in the presence of a perpendicular magnetic field, H . We find significant differences in the phase diagrams in the magnetic field–temperature plane between three-dimensional (3D) and 2D NbN films. The differences are most striking close to the normal-superconductor phase transition. We establish that these variances have their origin in the differing pinning properties in two different dimensions. We obtain the pinning strength quantitatively in both the dimensions from two independent transport measurements performed in two different regimes of vortex motion: (i) thermally assisted flux-flow regime and (ii) flux flow regime. Both the measurements consistently show that both the pinning potential and the zero-field free-energy barrier to depinning in the 3D superconductor are at least an order of magnitude stronger than that in the 2D superconductor. Further, we probed the dynamics of pinning in both 2D and 3D superconductor through voltage fluctuation spectroscopy. We find that the mechanism of vortex pinning–depinning is qualitatively similar for the 3D and 2D superconductors. The voltage-fluctuations arising from vortex motion are found to be correlated only in the 2D superconductor. We establish this to be due to the presence of long-range phase fluctuations near the Berezinskii-Kosterlitz-Thouless–type superconducting transition in 2D superconductors.

DOI: [10.1103/PhysRevB.100.174501](https://doi.org/10.1103/PhysRevB.100.174501)**I. INTRODUCTION**

Beyond the lower critical field (H_{C1}), magnetic field penetrates a type-II superconductor (SC) in the form of topological defects known as vortices or fluxoids [1]. A vortex comprises a circulating supercurrent and encloses a magnetic flux quantized to $\phi_0 = h/(2e)$. The interaction between the vortices is repulsive, producing a periodic structure called the Abrikosov vortex lattice (VL) [2,3]. The periodicity of this lattice gets distorted in the presence of inhomogeneities and fluctuations (both thermal and quantum) having energy scales comparable to the elastic energy of the VL [4–10]. For a disordered superconductor, the phase diagram is complex. Depending on the relative strengths of the pinning-potential, thermal energy, and elastic energy of the VL, a gamut of phases like vortex-solid, vortex-fluid, and vortex-glass can exist [5,11,12]. Several different types of phase transitions/crossovers connecting these phases have been predicted (and in some cases experimentally verified) in a three-dimensional superconductor (3D-SC) [12–16]. The phase diagram becomes even more interesting in a 2D-SC in which even for arbitrarily small pinning strengths, the long-range translational order of the VL is lost although rotational order survives [11,12,17–22]. Thus an understanding of the interplay of fluctuations, disorder, and dimensionality is of paramount importance in describing the dynamics and the related phase transitions of the vortex state of a type-II SC.

In an idealized SC devoid of defects, the vortices are free, and an infinitesimal current or thermal excitation is enough to cause them to move leading to dissipation [23]. Thus, in such a system, in the presence of a magnetic field, the true zero-resistance state can survive only at zero temperature. Vortex pinning is essential to restore the zero-resistance state in a disordered SC. Hence, an understanding of pinning mechanisms, methods to controllably create defects with high pinning potential or to produce commensurable pinning effects using artificially created ordered series of defects, has always been at the forefront of fundamental as well as applied research [24–29].

Among the many exciting features of high- T_C SC, pinning of vortices in the mixed state has always attracted much interest [15,30–36]. Even after decades of research, its exact origin and consequences are not well understood [12]. This is partly due to the complications present in high- T_C materials due to substantial thermal fluctuations or the “irreversibility-line” in the H - T phase diagram [37]. To circumvent these impediments, we probed the vortex lattice, both in 2D and 3D limits, in a conventional type-II superconductor. Specifically, we looked at thin films of NbN which are known to be in the strong-pinning limit [38–40]. The aim was to isolate and investigate only the dimensional effects on vortex dynamics. Local probes like scanning tunneling microscopy (STM) or magnetic force microscopy correlate the static position of the vortices with atomic-scale structural defects [41–44]. Magnetotransport measurements, on the other hand, probe the variation in the global dynamics of vortices with pinning potential strength or with dimensionality [12,20]. These two

*aveek@iisc.ac.in

complementary techniques together provide a detailed picture of local pinning forces as well as the collective dynamics of vortices. In a series of previous publications, some of us looked in detail, using low-temperature STM, at the local-dynamics of vortices in SC [38,40,45–47]. In this article, we look at the temporal and spatial correlations of the vortex dynamics through detailed magnetotransport measurements.

II. SAMPLE DETAILS AND MEASUREMENT SCHEMES

Bulk NbN is a well known, *s*-type, conventional type-II superconductor well described by Bardeen-Cooper-Schrieffer (BCS) theory [38,48]. High-quality NbN superconducting films of different thickness and desired disorder levels can be grown with excellent control [46,49]. This makes NbN an ideal system to compare and contrast superconductivity in two different dimensions—3D and 2D. The superconducting coherence length obtained from critical field measurement is ~ 6 nm for NbN; any NbN film of thickness less than 6 nm behaves as a 2D superconductor [47].

We studied the superconductor-normal phase diagram in the perpendicular magnetic field–temperature (H - T) plane for NbN films of two thicknesses: 68 nm (3D-SC) and 3 nm (2D-SC). The films were patterned into four-probe configurations, with four 10-nm/60-nm Cr/Au electrical contacts, each 2 mm wide and 1 mm in length and separated from each other by 200 μm and thermally deposited on them through a metal mask. The measurements were done in a pumped 2 K cryostat (equipped with an 8-T superconducting magnet) with the films immersed in the ^4He exchange gas to ensure good thermalization. Special care was taken to thermalize and low-pass filter the measurement wires (with a cut-off frequency of 500 kHz) going into the cryostat.

III. RESULTS AND DISCUSSIONS

The resistive transitions are found to be strikingly different in these two cases. We find that in 2D-SC, close to the Berezinsky-Kosterlitz-Thouless (BKT) transition [50,51] temperature T_{BKT} , a very small magnetic field is enough to give rise to dissipative transport even in the limit of vanishingly small current. In contrast, for the 3D-SC, a finite magnetic field is required to get dissipative transport over the entire phase space. In both cases, we have defined the critical temperature to be the T at which the sample resistance R becomes 1% of its normal state resistance R_N . To understand this significant difference in the response of superconductivity in different dimensions to a perpendicular magnetic field (H), we analyzed the pinning properties of vortices of both 2D- and 3D-SC. We conclude from two independent sets of measurements—(a) temperature dependence of the magnetoresistance and (b) H dependence of the critical current density J_C —that pinning of vortices is more than one order of magnitude stronger in 3D-SC than in 2D-SC. To understand the dynamical process of pinning of vortices, we looked into voltage fluctuations in these films as a function of H at temperatures close to T_C . We find that the voltage fluctuations are an order of magnitude slower in 2D-SC as compared to the 3D-SC. We also find that the dependence of the relative variance of voltage fluctuations on H is the same in both cases

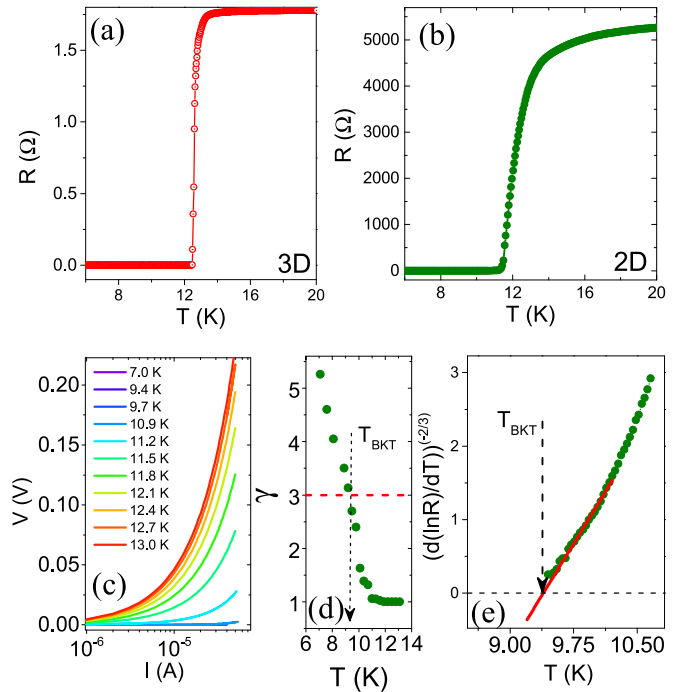


FIG. 1. Resistance versus temperature plot for the (a) 68-nm- and (b) 3-nm-thick NbN films. (c) Plots of the nonlinear current-voltage characteristics of the 3-nm NbN film at several temperatures around T_{BKT} . (d) Plot of γ versus temperature. $\gamma(T_{\text{BKT}}) = 3$ is marked by red dashed line; this yields $T_{\text{BKT}} = 9.4$ K. (e) Fit of the measured temperature dependence of resistance to Eq. (1). The green filled circles are the data and the solid red line is the fit. T_{BKT} extracted from the intercept is found to be 9.4 K.

showing that pinning-depinning of vortices is the dominant source of noise in both 2D- and 3D-SC. Computations of higher moments of fluctuations indicate the presence of strong correlations between the vortex motion in 2D while it is essentially uncorrelated in the 3D-SC.

Figure 1(a) shows the temperature dependence of the resistance of the 3D-SC NbN film. The mean-field transition temperature T_C for this film is 12.4 K. The corresponding data for the 3-nm film are plotted in Fig. 1(b). Our previous studies of the temperature dependence of superfluid density have established that the 3-nm-thick NbN film undergoes a BKT transition (which is a hallmark of 2D-SC) while the 68-nm film is a BCS 3D-SC [47–49]. In this paper, we employ a different approach and identify T_{BKT} for the 3-nm NbN superconducting film from electrical transport measurements. One can identify T_{BKT} by two different electrical transport measurements. The first comes from the measurements of current-voltage (I - V) characteristics in the superconducting regime. According to a Ginzburg-Landau Coulomb gas description of 2D-SC, a finite driving electrical current flowing through the sample leads to proliferation of free vortices from dissociation of bound vortex-antivortex pairs. These freely flowing vortices cause phase-slips giving rise to dissipation in the system which follows, in the low-current range, a nonlinear I - V relation: $V \sim I^\gamma$ [19,30,52–55]. In this prescription, T_{BKT} is identified by the criterion $\gamma(T_{\text{BKT}}) = 3$. The I - V characteristics measured at different T are plotted in Fig. 1(c).

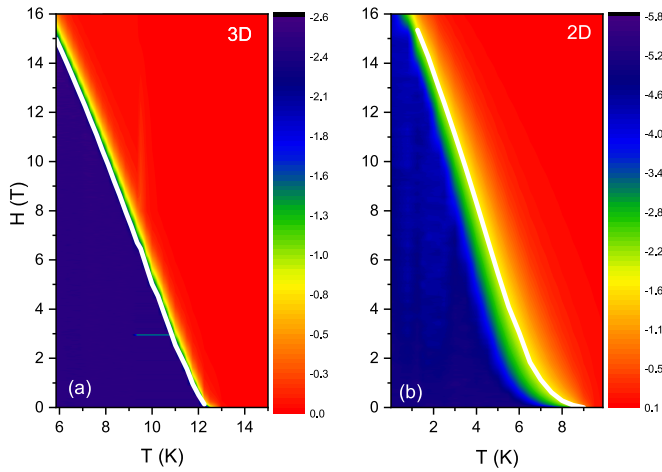


FIG. 2. (a) Plot of the logarithm of the normalized resistance, $\log(R/R_N)$, in the H - T plane for the 3D-SC. (b) Corresponding plot for the 2D-SC. The solid white line in both the plots show the H_C [defined as $R(T, H = H_C) = 0.01R_N$] as a function of T .

The corresponding γ values are plotted in Fig. 1(d). From this plot, we identify T_{BKT} to be ~ 9.4 K.

The second method to obtain T_{BKT} is from the temperature dependence of resistance R of the SC. Near T_{BKT} , for a 2D-SC, it is known to follow the relation:

$$R = R_0 \exp \left[\frac{b_R}{(T - T_{\text{BKT}})^{1/2}} \right], \quad (1)$$

where b_R is a measure of the strength of interaction between the vortices and antivortices [30,56,57]. In this temperature regime vortex-antivortex pairs unbind thermally. Their proliferation leads to phase fluctuations and consequently to the suppression of superconductivity. To estimate T_{BKT} , we fit the R - T data to Eq. (1) as shown in Fig. 1(e). This procedure yields $T_{\text{BKT}} \sim 9.4$ K, which is in agreement with T_{BKT} extracted from nonlinear I - V characteristics. This value of T_{BKT} also matches closely with that obtained from measurements of superfluid number-density by us [45,47]. Note that this method is an approximation and is not compelling enough to establish the two-dimensional nature of superconductivity. The important drawbacks of this method are as follows: (i) finite-size effects are ignored and (ii) it is valid over a very narrow temperature range $T_{\text{BKT}} \leq T < T_C$. Nonetheless, it is a handy technique to estimate the BKT transition temperature in materials where the 2D nature of SC is already established.

We now turn to the response of the superconducting state to a magnetic field H applied perpendicularly to the plane of the film. We obtain the phase diagram in the H - T plane from magnetoresistance measurements performed at different temperatures. The phase diagrams are shown in Figs. 2(a) and 2(b) for 3D-SC and the 2D-SC, respectively. There is a significant difference in the way dissipation arises close to transition temperature in these two cases. For example, at $T = 0.85 T_C$ for 3D-SC 4.12 T is needed to get finite dissipation. On the other hand, an order-of-magnitude-smaller field (~ 0.44 T) is enough to induce dissipative transport in the 2D-SC at $T = 0.85 T_C$. A possible reason for this fragility of SC in 2D as compared to its 3D counterpart can be the

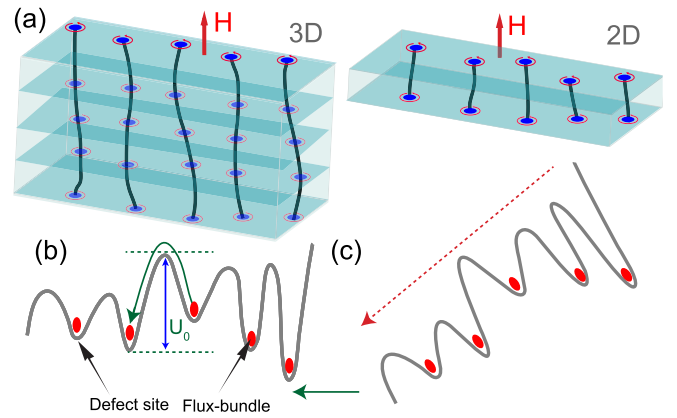


FIG. 3. (a) Schematic showing the difference in pinning strengths between 3D-SC and 2D-SC. (b) Schematic illustrating the concept of vortices getting pinned at local pinning-potential minima at $J \ll J_C$. The free-energy barrier to hop from one pinning-site to another is $U_0(H)$. The vortices can only hop from one pinning-site to another by thermal activation—this is the thermally activated flux flow (TAFF) regime. (c) In the presence of a driving current $J \geq J_C$ through the SC, the Lorentz-force lowers the hopping barrier by effectively tilting the potential landscape. When $\mathbf{F}_L(H) \geq \mathbf{F}_P(H)$, the vortices can flow freely giving rise to an increase in dissipation—this is the flux flow (FF) regime.

difference in pinning strength of vortices in the two cases. In ultrathin 2D films, the vortices are effectively pancake-like as opposed to the tubelike structure in 3D. Consequently, in 3D-SC the vortices naturally get pinned at several different pinning sites along the thickness of the film. The pancake vortices in 2D-SC do not get pinned as much and hence can move more easily, giving rise to dissipation. The idea is illustrated in Fig. 3(a) which represents schematically the pinning in 3D-SC and 2D-SC.

To test this hypothesis of differing pinning strengths in 2D-SC and 3D-SC, we estimated the pinning force and pinning energy from two independent measurements in both 2D and 3D superconductors. Transport measurements evaluate the average pinning force on vortices considering the pinning of the flux-bundles due to sample inhomogeneities and also the interaction between the vortices. For values of magnetic fields much smaller than the upper-critical field, $H \ll H_{C2}$, the vortices are separated by large distances $\sim \sqrt{H/\phi_0}$ as compared to the penetration depth, λ . In this limit, the vortices can be considered as independent, noninteracting objects. Recall that a current density $\mathbf{J}(\mathbf{H})$ flowing through the SC perpendicular to the magnetic field \mathbf{H} leads to a Lorentz force $\mathbf{F}_L(H) = d_{\text{film}} \mathbf{J} \times \hat{\mathbf{n}} \phi_0$ acting on each vortex line. Here $\hat{\mathbf{n}}$ is the unit vector parallel to \mathbf{H} , d_{film} is the film thickness, and $\phi_0 = h/(2e)$ is the flux quantum, which is the net flux threading a single vortex. This force tends to aid the flux bundles overcome the free-energy barriers related to the pinning effect of inhomogeneities in the sample and move them in a direction perpendicular to both \mathbf{J} and \mathbf{H} . It is opposed by the average pinning force per vortex, $\mathbf{F}_P(H)$, leading to the net force on the vortex being $\mathbf{F}_{\text{net}}(H) = \mathbf{F}_L(H) + \mathbf{F}_P(H) = d_{\text{film}} \mathbf{J}(\mathbf{H}) \times \hat{\mathbf{n}} \phi_0 + \mathbf{F}_P(H)$. When the Lorentz force overcomes the pinning force, the

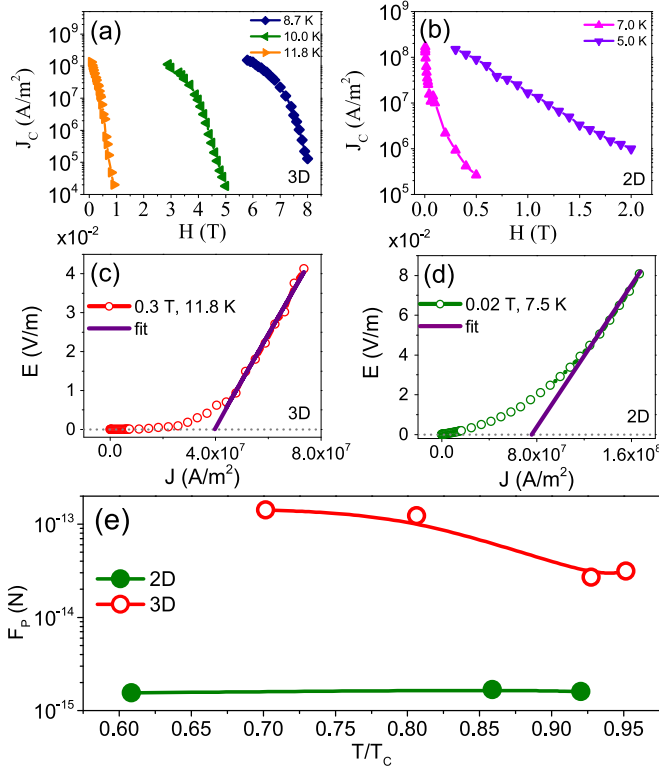


FIG. 4. (a) Plots showing the variation of critical current density J_C versus the magnetic field H at few selected temperatures for the 3D-SC. (b) Plot of the corresponding data for the 2D-SC. (c) Plot of E versus J for the 3D-SC measured at $T/T_C = 0.95$ and $H = 0.3$ T. (d) Plot of E versus J for the 2D-SC measured at $T/T_{BKT} = 0.9$ and $H = 0.02$ T. The intercept of the solid purple lines in both (c) and (d) give the value of corresponding J_C . (e) Plot of pinning force per vortex F_P versus T/T_C . One can see that the F_P in 3D-SC is at least an order of magnitude stronger than in the 2D-SC.

vortices get depinned and begin to flow. This motion induces an electric potential in a direction perpendicular to both \mathbf{H} and \mathbf{F}_L , i.e., in a direction parallel to \mathbf{J} . Thus, work is done, and energy is dissipated—the vortex motion leads to a finite resistance. The critical-current density \mathbf{J}_C is defined as the maximum current density that can flow through the SC without depinning the vortices or, equivalently, $\lim_{H \rightarrow 0} \mathbf{F}_{\text{net}}(H) = 0$. This force-balance equation relates the maximum magnitude of the pinning force to that of the critical current density:

$$F_P(H) = d_{\text{film}} J_C \phi_0. \quad (2)$$

The limit $H \rightarrow 0$ ensures that the interactions between the vortices are irrelevant.

We obtained $J_C(H)$ as a function of H from measurements of J versus E at different T and H . J_C was defined operationally as the value of current density at which the potential drop across the film equaled 1 mV/m. The measured variation of J_C with H is shown in Fig. 4(a) and Fig. 4(b) for the 3D- and 2D-SC, respectively.

The value of $J_C(H)$ were also extracted using an alternate independent method, by defining it to be the value of J at which the linear-fit to the E - J plots intersects the J axis, here E is the electric field in the plane of the film [see Figs. 4(c)

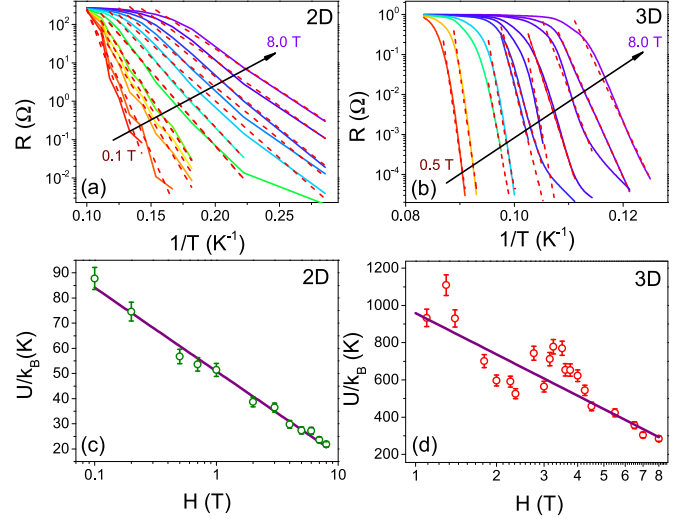


FIG. 5. [(a) and (b)] Plots of R , in log scale, versus $1/T$ at different magnetic fields for the 2D-SC and 3D-SC, respectively. The red dashed lines in both the plots are the Arrhenius fits. The measurements were all performed in the TAFF regime. (c) The green open circles are the extracted activation energies $U(H)$ as a function of H for the 2D-SC. The purple line is the fit to the relation $U(H) = U_0 \ln(H_0/H)$, yielding $U_0/k_B = 14.5$ K. (d) $U(H)$ for the 3D-SC has a nonmonotonic dependence on H for the 3D-SC. The purple lines is a plot of the relation $U(H) = U_0 \ln(H_0/H)$ with $U_0/k_B = 280$ K.

and 4(d) for representative plots]. The validity of this method stems from the fact that above $J > J_C$, the flux-flow (FF) regime sets in, and resistance in this regime, $R_{\text{FF}}(H)$, is independent of the current; hence the E - J curve is linear. These two independent methods give values of $J_C(H)$ which match within a factor of 2 to 3.

The average pinning force on each vortex-line $F_P(H)$ was calculated using Eq. (2); the results are plotted in Fig. 4(e). It is observed that vortex pinning strength for the 3D-SC is more than an order of magnitude larger than that for the 2D-SC. This is in agreement with our observation of initiation of dissipation in 2D-SC at much smaller values of H as compared to the 3D-SC.

The pinning strength can also be determined from the temperature T dependence of the resistance of SC at $J \ll J_C$ in the presence of H . At such low current densities, $F_L \ll F_P$ and flux motion can take place only through thermal activation over the free-energy barriers related to the pinning induced by inhomogeneities in the sample. This regime is known as thermally activated flux flow (TAFF). The idea is illustrated in Fig. 3(b). The differential resistance in this regime, R_{TAFF} has a thermally activated behavior: $\lim_{J \rightarrow 0} R_{\text{TAFF}}(T, H) = R_0 \exp[-U(H)/k_B T]$, where $U(H)$ is the energy scale of the zero-field free-energy barrier to depinning [20,58,59]. Figures 5(a) and 5(b) show plots of R in log scale as a function of $1/T$ at different H for 2D- and 3D-SC, respectively; the slopes of these plots give $U(H)$. The red dashed lines are the linear fits to the data. Note that in our measurements, this activated behavior is observed over four decades in resistance. Figure 5(c) shows a plot of $U(H)$ versus H for the 2D-SC in a semilog scale; the data were found to follow a logarithmic relation $U(H) = U_0 \ln(H_0/H)$ with $U_0/k_B \sim 14.5$ K.

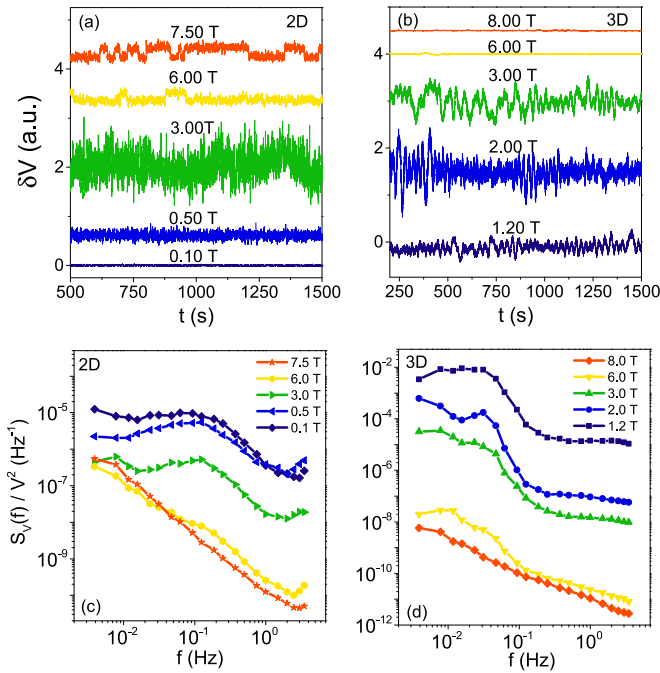


FIG. 6. [(a) and (b)] Plots of the time series of voltage fluctuations at selected values of the magnetic field H for the 2D- and 3D-SC, respectively. The data have been vertically shifted for clarity. [(c) and (d)] Plots of the normalized power spectral density of voltage fluctuations at the corresponding H for 2D- and 3D-SC, respectively.

Theory predicts this logarithmic dependence of $U(H)$ on H in the TAFF region with $U_0 = \frac{\phi_0^2 d}{256\pi^3 \lambda^2}$ [20,59]. For NbN, $\lambda \approx 500$ nm giving estimated U_0/k_B to be ~ 20 K for 3-nm-thick NbN SC which agrees very well with our experimentally obtained number.

Figure 5(d) shows that, unlike the case of 2D-SC, $U(H)$ for the 3D-SC varies with H in a nonmonotonic fashion. The purple line is a plot of $U(H) = U_0 \ln(H_0/H)$ with $U_0/k_B = 280$ K. The line matches the general trend of the plot of $U(H)/k_B$ versus H showing that U_0 is approximately an order of magnitude larger in 3D-SC than its 2D counterpart. The nonmonotonic dependence of $U(H)$ on H has been observed previously in a similar superconducting system, thin-films of $\text{Mo}_x\text{Ge}_{1-x}$ [20]. To the best of our knowledge, there is no well-accepted explanation for this phenomenon. On comparison, we find that the activation energy scale $U(H)$ extracted from R - T plot is ~ 10 times larger for the 3D-SC as compared to the 2D-SC. This observation is consistent with our estimate of comparative pinning forces in the two dimensions [Fig. 4(e)]. Using these two quantities [$F_p(H)$ and $U(H)$], we can estimate the spatial range of the pinning potential (which one can heuristically equate to the separation between pinning sites) to be ~ 100 nm for both 2D- and 3D-SC which roughly equals the impurity distribution in our films.

Thermally activated pinning-depinning of vortices from sample inhomogeneities is a stochastic, dynamic process. As vortex motion gives rise to resistance in SC, a careful study of the dynamics of resistance fluctuations or, equivalently, voltage fluctuations when the sample is driven by a with constant

current should provide insights into vortex fluctuations. This motivated us to study voltage fluctuation and its higher-order moments in both 2D-SC and 3D-SC at a fixed temperature $T = 0.95 T_C$ for the 3D-SC ($T = 0.97 T_{\text{BKT}}$ for the 2D-SC) and at various values of the perpendicular magnetic field H .

To probe the voltage fluctuations (noise) and its statistics, we used a digital signal processing-based technique [60,61]. The technique allows us to measure the background noise as well as the dynamical noise from the sample at the same time. The film was biased by an ac current density $J \ll J_C$.

Plots of the voltage-fluctuation time series for the 2D-SC and 3D-SC at a few selected values of H are shown in Figs. 6(a) and 6(b). The normalized power spectral density (PSD) of voltage fluctuations, $S_V(f)/V^2$ for the 2D-SC and 3D-SC at the corresponding values of H are plotted in Figs. 6(c) and 6(d), respectively. For fields $H > H_{C2}$, the dependence of $S_V(f)$ on f , in both 2D- and 3D-SC, was found to be $S_V(f) \propto 1/f^\alpha$, where $\alpha \sim 1.1$. On the other hand, for $H < H_{C2}$, $S_V(f)$ was found to have developed a significant hump at a specific frequency f_c riding on top of the $1/f^\alpha$ noise; f_c for the 2D-SC and the 3D-SC were ~ 0.125 and 0.012 Hz, respectively. This significant difference in the characteristic frequency scale of voltage fluctuations in 2D-SC and 3D-SC is a consequence of the fact that the pinning potential in the 2D-SC is significantly stronger than that in 3D.

The PSD of voltage fluctuation can be integrated over the bandwidth of measurement to obtain the variance of voltage fluctuations \mathcal{V}_{var} [61]:

$$\mathcal{V}_{\text{var}} \equiv \langle \delta V^2 \rangle = \int_{0.004\text{Hz}}^{4\text{Hz}} S_V(f) df. \quad (3)$$

Figure 7(a) show plots of \mathcal{V}_{var} as a function of H . In both 2D- and 3D-SC, we observe that the variance peaks around the same value of the magnetic field, $H \sim 2$ T. A probable origin of this noise can be fluctuations in H as dV/dH is quite sharp in this regime [Fig. 7(b)]. We rule out this trivial explanation by noting that the maximum voltage fluctuations arising from fluctuations in the magnetic field, δH , can be $\mathcal{V}_{\text{var}}^{\text{mag}}(H) = [(dV/dH)\delta H]^2$. In our system the maximum value of δH was measured to be 9×10^{-5} T. Using this value, we estimate the noise due to H -field fluctuations at $H = 2$ T to be $\sim 10^{-16}$ V^2 for the 2D-SC; this value is at least two orders of magnitude smaller than the measured \mathcal{V}_{var} at 2 T.

Instead, we propose that the observed noise arises from dynamic trapping-detrapping of vortices. The peak in the variance of voltage fluctuations for both 2D-SC and 3D-SC NbN films appear at the same magnetic field, indicating that the magnitude of voltage fluctuations depends only on the number of vortices and not on the dimensionality of the system. Recall that the current density used during the noise measurements are minimal ($J \ll J_C$) and so the transport is by thermal activation of vortices. Consider then the following scenario: At low H , there are very few vortices. Consequently, both the voltage drop V (caused by phase slips due to vortex-drift under the driving current, hence proportional to the number of free vortices) and the voltage-fluctuations \mathcal{V}_{var} (caused by fluctuation in the number of such phase-slip events, i.e., proportional to the variance in the number-density of free

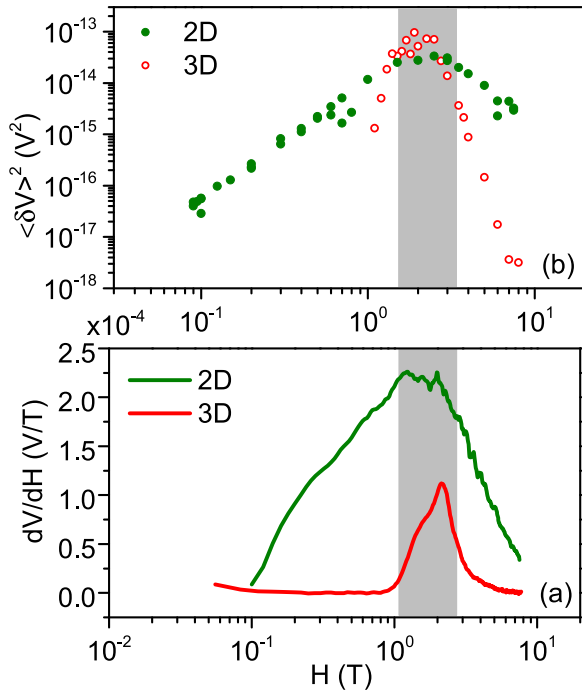


FIG. 7. (a) Variance of voltage fluctuations \mathcal{V}_{var} versus applied perpendicular magnetic field H for 2D-SC (green filled circles) and 3D-SC (red open circles). (b) Plot of dV/dH versus H for 2D-SC (dotted green line) and 3D-SC (solid red line). The gray shaded area indicates the range of the magnetic field where the noise peaks for both 2D-SC and 3D-SC.

vortices) are small. As H increases, both V and \mathcal{V}_{var} increase as there are more vortices available to take part in these processes. Beyond a certain field, almost all the pinning sites get accommodated with vortices, and there are not enough

vacant pinning sites for the vortices to hop to; the fluctuations in the number of free vortices and consequently the voltage fluctuations decrease.

IV. CONCLUSION

To conclude, in this article, we have explored the differences in vortex dynamics in two-dimensional and three-dimensional superconductors. Our studies were performed on thin films of the same material system (NbN) prepared under identical conditions, thus eliminating the possibility of material-specific artifacts in comparison across dimensions, an issue that has plagued the community for a long time. We established that the observed fragility of 2D-SC to a perpendicular magnetic field as compared to the 3D-SC stems from the differing pinning properties in these two dimensions. We show, from two independent transport measurements carried out in two different regimes of vortex dynamics, that both the pinning strength and the free-energy barrier to depinning are at least an order of magnitude stronger in 3D-SC than in 2D-SC. From voltage fluctuation measurements, we find that the dynamic process of flux pinning depinning is similar in both 2D and 3D.

ACKNOWLEDGMENTS

A.B. acknowledges financial support from Nanomission, DST, Government of India, Project No. SR/NM/NS-35/2012; SERB, DST, Government of India, and Indo-French Centre for the Promotion of Advanced Research (CEFIPRA). P.R. acknowledges funding from the Department of Atomic Energy. H.K.K. thanks CSIR, MHRD, Government of India, for financial support. We acknowledge Vivas Bagwe for technical help in sample preparation.

- [1] M. Tinkham, *Introduction to Superconductivity* (Dover Publication, New York, 2004).
- [2] A. Abrikosov, *J. Phys. Chem. Solids* **2**, 199 (1957).
- [3] L.-P. Levy, *Vortices in Type II Superconductor: Magnetism and Superconductivity: Texts and Monographs in Physics* (Springer Science & Business Media, New York, 2013).
- [4] T. Nattermann and S. Scheidl, *Adv. Phys.* **49**, 607 (2000).
- [5] M. J. Higgins and S. Bhattacharya, *Physica C* **257**, 232 (1996).
- [6] T. Giamarchi and P. Le Doussal, *Phys. Rev. B* **52**, 1242 (1995).
- [7] T. Giamarchi and P. Le Doussal, *Phys. Rev. B* **55**, 6577 (1997).
- [8] S. C. Ganguli, H. Singh, G. Saraswat, R. Ganguly, V. Bagwe, P. Shirage, A. Thamizhavel, and P. Raychaudhuri, *Sci. Rep.* **5**, 10613 (2015).
- [9] S. Sengupta, C. Dasgupta, H. R. Krishnamurthy, G. I. Menon, and T. V. Ramakrishnan, *Phys. Rev. Lett.* **67**, 3444 (1991).
- [10] A. De Col, G. I. Menon, and G. Blatter, *Phys. Rev. B* **75**, 014518 (2007).
- [11] D. S. Fisher, M. P. A. Fisher, and D. A. Huse, *Phys. Rev. B* **43**, 130 (1991).
- [12] G. Blatter, M. V. Feigel'man, V. B. Geshkenbein, A. I. Larkin, and V. M. Vinokur, *Rev. Mod. Phys.* **66**, 1125 (1994).
- [13] I. Roy, S. Dutta, A. N. Roy Choudhury, S. Basistha, I. Maccari, S. Mandal, J. Jesudasan, V. Bagwe, C. Castellani, L. Benfatto, and P. Raychaudhuri, *Phys. Rev. Lett.* **122**, 047001 (2019).
- [14] E. Herrera, J. Benito-Llorens, U. S. Kaluarachchi, S. L. Bud'ko, P. C. Canfield, I. Guillamón, and H. Suderow, *Phys. Rev. B* **95**, 134505 (2017).
- [15] R. H. Koch, V. Foglietti, W. J. Gallagher, G. Koren, A. Gupta, and M. P. A. Fisher, *Phys. Rev. Lett.* **63**, 1511 (1989).
- [16] B. Khaykovich, E. Zeldov, D. Majer, T. W. Li, P. H. Kes, and M. Konczykowski, *Phys. Rev. Lett.* **76**, 2555 (1996).
- [17] B. I. Halperin and D. R. Nelson, *Phys. Rev. Lett.* **41**, 121 (1978).
- [18] A. I. Larkin and Y. N. Ovchinnikov, *J. Low Temp. Phys.* **34**, 409 (1979).
- [19] A. Tsen, B. Hunt, Y. Kim, Z. Yuan, S. Jia, R. J. Cava, J. Hone, P. Kim, C. Dean, and A. Pasupathy, *Nat. Phys.* **12**, 208 (2016).
- [20] W. R. White, A. Kapitulnik, and M. R. Beasley, *Phys. Rev. Lett.* **70**, 670 (1993).
- [21] M. P. A. Fisher, *Phys. Rev. Lett.* **65**, 923 (1990).
- [22] A. Benyamini, E. J. Telford, D. M. Kennes, D. Wang, A. Williams, K. Watanabe, T. Taniguchi, J. Hone, C. Dean, A. Millis *et al.*, *Nat. Phys.* **115**, 947 (2019).
- [23] J. Bardeen and M. J. Stephen, *Phys. Rev.* **140**, A1197 (1965).

- [24] J. E. Villegas, S. Savel'ev, F. Nori, E. M. Gonzalez, J. V. Anguita, R. García, and J. L. Vicent, *Science* **302**, 1188 (2003).
- [25] A. Hoffmann, L. Fumagalli, N. Jahedi, J. C. Sautner, J. E. Pearson, G. Mihajlović, and V. Metlushko, *Phys. Rev. B* **77**, 060506(R) (2008).
- [26] T. Shapoval, V. Metlushko, M. Wolf, B. Holzapfel, V. Neu, and L. Schultz, *Phys. Rev. B* **81**, 092505 (2010).
- [27] B. Y. Zhu, F. Marchesoni, and F. Nori, *Phys. Rev. Lett.* **92**, 180602 (2004).
- [28] C. C. de Souza Silva, A. V. Silhanek, J. Van de Vondel, W. Gillijns, V. Metlushko, B. Ilic, and V. V. Moshchalkov, *Phys. Rev. Lett.* **98**, 117005 (2007).
- [29] C. Reichhardt, C. J. Olson, and F. Nori, *Phys. Rev. Lett.* **78**, 2648 (1997).
- [30] P. Minnhagen, *Rev. Mod. Phys.* **59**, 1001 (1987).
- [31] M. Feigel'man, V. Geshkenbein, and A. Larkin, *Physica C* **167**, 177 (1990).
- [32] V. M. Vinokur, M. V. Feigel'man, V. B. Geshkenbein, and A. I. Larkin, *Phys. Rev. Lett.* **65**, 259 (1990).
- [33] T. Worthington, F. Holtzberg, and C. Feild, *Cryogenics* **30**, 417 (1990).
- [34] W. K. Kwok, U. Welp, G. W. Crabtree, K. G. Vandervoort, R. Hulscher, and J. Z. Liu, *Phys. Rev. Lett.* **64**, 966 (1990).
- [35] C. J. van der Beek, M. Konczykowski, A. Abal'oshev, I. Abal'osheva, P. Gierlowski, S. J. Lewandowski, M. V. Indenbom, and S. Barbanera, *Phys. Rev. B* **66**, 024523 (2002).
- [36] F. C. Klaassen, G. Doornbos, J. M. Huijbregtse, R. C. F. van der Geest, B. Dam, and R. Griessen, *Phys. Rev. B* **64**, 184523 (2001).
- [37] Y. Yeshurun and A. P. Malozemoff, *Phys. Rev. Lett.* **60**, 2202 (1988).
- [38] S. P. Chockalingam, M. Chand, A. Kamlapure, J. Jesudasan, A. Mishra, V. Tripathi, and P. Raychaudhuri, *Phys. Rev. B* **79**, 094509 (2009).
- [39] T. Shapoval, H. Stopfel, S. Haindl, J. Engelmann, D. S. Inosov, B. Holzapfel, V. Neu, and L. Schultz, *Phys. Rev. B* **83**, 214517 (2011).
- [40] R. Ganguly, I. Roy, A. Banerjee, H. Singh, A. Ghosal, and P. Raychaudhuri, *Phys. Rev. B* **96**, 054509 (2017).
- [41] O. M. Auslaender, E. W. J. Luan, Lan Straver, J. E. Hoffman, N. C. Koshnick, E. Zeldov, D. A. Bonn, R. Liang, W. N. Hardy, and K. A. Moler, *Nat. Phys.* **5**, 35 (2008).
- [42] F. Pardo, F. de la Cruz, P. L. Gammel, E. Bucher, and D. J. Bishop, *Nature* **396**, 348 (1998).
- [43] J. E. Hoffman, K. McElroy, D.-H. Lee, K. M. Lang, H. Eisaki, S. Uchida, and J. C. Davis, *Science* **297**, 1148 (2002).
- [44] O. Fischer, M. Kugler, I. Maggio-Aprile, C. Berthod, and C. Renner, *Rev. Mod. Phys.* **79**, 353 (2007).
- [45] M. Mondal, S. Kumar, M. Chand, A. Kamlapure, G. Saraswat, G. Seibold, L. Benfatto, and P. Raychaudhuri, *Phys. Rev. Lett.* **107**, 217003 (2011).
- [46] M. Chand, G. Saraswat, A. Kamlapure, M. Mondal, S. Kumar, J. Jesudasan, V. Bagwe, L. Benfatto, V. Tripathi, and P. Raychaudhuri, *Phys. Rev. B* **85**, 014508 (2012).
- [47] R. Koushik, S. Kumar, K. R. Amin, M. Mondal, J. Jesudasan, A. Bid, P. Raychaudhuri, and A. Ghosh, *Phys. Rev. Lett.* **111**, 197001 (2013).
- [48] M. Mondal, A. Kamlapure, M. Chand, G. Saraswat, S. Kumar, J. Jesudasan, L. Benfatto, V. Tripathi, and P. Raychaudhuri, *Phys. Rev. Lett.* **106**, 047001 (2011).
- [49] R. Ganguly, D. Chaudhuri, P. Raychaudhuri, and L. Benfatto, *Phys. Rev. B* **91**, 054514 (2015).
- [50] J. Kosterlitz and D. Thouless, *J. Phys. C* **6**, 1181 (1972).
- [51] V. Berezinski, *JETP* **32**, 493 (1971).
- [52] N.-C. Yeh and C. C. Tsuei, *Phys. Rev. B* **39**, 9708 (1989).
- [53] Q. Y. Ying and H. S. Kwok, *Phys. Rev. B* **42**, 2242 (1990).
- [54] G. N. Daptary, S. Kumar, P. Kumar, A. Dogra, N. Mohanta, A. Taraphder, and A. Bid, *Phys. Rev. B* **94**, 085104 (2016).
- [55] N. Reyren, S. Thiel, A. D. Caviglia, L. F. Kourkoutis, G. Hammerl, C. Richter, C. W. Schneider, T. Kopp, A.-S. Rüetschi, D. Jaccard, M. Gabay, D. A. Muller, J.-M. Triscone, and J. Mannhart, *Science* **317**, 1196 (2007).
- [56] D. Finotello and F. M. Gasparini, *Phys. Rev. Lett.* **55**, 2156 (1985).
- [57] V. Ambegaokar, B. I. Halperin, D. R. Nelson, and E. D. Siggia, *Phys. Rev. B* **21**, 1806 (1980).
- [58] T. T. M. Palstra, B. Batlogg, L. F. Schneemeyer, and J. V. Waszczak, *Phys. Rev. Lett.* **61**, 1662 (1988).
- [59] O. Brunner, L. Antognazza, J.-M. Triscone, L. Miéville, and O. Fischer, *Phys. Rev. Lett.* **67**, 1354 (1991).
- [60] J. H. Scofield, *Rev. Sci. Instr.* **58**, 985 (1987).
- [61] A. Bid, Resistance fluctuations and instability in metal nanowires, Ph.D. thesis, Indian Institute of Science, 2006.